Geomechanics and Engineering, *Vol. 31, No. 5 (2022) 519-527*
https://doi.org/10.12989/gae.2022.31.5.519

Effect of water distribution on shear strength of compacted loess

Kang-ze Yuan[1,2], Wan-kui Ni*[1], Xiang-fei Lü**[1] and Hai-man Wang[1]

[1]*Department of Geological Engineering, College of Geological Engineering and Surveying and Mapping, Chang'An University, No.126 Yanta Road, Xi'an, Shaanxi 710054, P.R. China*
[2]*Department of Civil and Environmental Engineering, Politecnico di Milano, Piazza Leonardo da Vinci, 32, 20133 Milano, Italy*

(*Received June 26, 2021, Revised October 21, 2022, Accepted December 5, 2022*)

Abstract. Shear failure in soil is the primary cause of most geotechnical structure failures or instability. Soil water content is a significant factor affecting soil shear strength. In this study, the shear strength of samples with different water contents was tested. The shear strength, cohesion, and internal friction angle decreased with increasing water content. Based on the variation of cohesion and internal friction angle, the water content zone was divided into a high-water content zone and low-water content zone with a threshold water content of 15.05%. Cohesion and internal friction angle have a good linear relationship with water content in both zones. Environmental Scanning Electron Microscopy (ESEM) test presented that the aggregates size of the compacted loess gradually increases with increasing water content. Meanwhile, the clay in the compacted loess forms a matric that envelops around the surface of the aggregates and fills the inter-aggregates pores. A quantitative analysis of bound water and free water under different water contents using a nuclear magnetic resonance (NMR) test was carried out. The threshold water content between bound water and free water was slightly below the plastic limit, which is consistent with the results of shear strength parameters. Combined with the T_2 distributions obtained by NMR, one can define a T_2 relaxation time of 1.58 ms as the boundary point for bound water distribution without free water. Finally, the effects of bound water and free water on shear strength parameters were analyzed using linear regression analysis.

Keywords: bound water; ESEM; linear regression analysis; loess; shear strength

1. Introduction

Loess deposits cover 10% of the world's continents, including Asia, Africa, central and southern Europe, the American Midwest, and northern France (Rost 2001, Pye 1995, Smalley and Rogers 1996). In northwestern China, Loess is extremely important and covers 630,000 km^2, primarily in the Shanxi, Shaanxi, Gansu, and Ningxia regions (Mei *et al.* 2016). Typical loess is considered to be an aeolian deposit with an open and meta-stable structure, which is characterized by high porosity, low density, loose accumulation, and strong collapsibility due to macropores. Therefore, loess foundation is prone to some engineering problems, including differential settlement, cracking, structural damage, and slope failure (Dijkstra *et al.* 1994, Sandra *et al.* 2001, Ahmed *et al.* 2013, Bakir *et al.* 2017). These engineering problems are related to soil mechanical properties, and soil shear strength is a key index for determining slope stability. When soil shear stress reaches its shear strength, the loess structure loses its stability (Markgraf 2006, Carey *et al.* 2016). In order to deal with and solve these problems effectively, studying the shear characteristics of loess is necessary, especially the influence of water content on the shear characteristics of loess (Kie *et al.* 1988, Derbyshire *et al.* 1994).

Significant research aimed at understanding the effect on shear strength of loess under different water contents has been carried out. Gu *et al.* (2019) performed direct shear tests and found that cohesion increased linearly with decreasing water content; whereas, the suction internal friction angle was approximately constant. The same experimental method was used to show that the cohesion and internal friction angle is inversely proportional to water content (Guo *et al.* 2021). Assallay *et al.* (1997) explored the shear strength of undisturbed loess as well as remolded loess and the undisturbed loess specimens a had larger effective cohesion but smaller internal friction angles compared to the corresponding remolded specimens. Consistent evidence has shown that for the same water content, the peak shear strength and strength parameters of remolded loess were significantly lower than those of undisturbed loess (Wen *et al.* 2013). Therefore, clarifying the effects of water content on soil shear strength is critical to understanding the mechanism of structural damage and slope failure.

Water in soil can be classified into bound water and free water (Low 1979). As clay particles in the water medium show charged characteristics, which forms an electric field around the particle and water molecules are polar molecules, positive and negative charges are distributed at both ends of water molecules. The cationic and polar water molecules are attracted around the particles within the electric field range and form a directional arrangement to form the bound water. The electric field attraction decreases with increasing distance. Free water is composed of water

*Corresponding author, Professor
E-mail: niwankui@chd.edu.cn
**Corresponding author, Professor
E-mail: lvxf@chd.edu.cn

ISSN: 2005-307X (Print), 2092-6219 (Online)

molecules not affected by electric field attraction. At present, the classification methods for bound water and free water primarily include X-ray diffraction, differential scanning calorimetry, centrifugal setting method, isothermal adsorption experiment (IAE), thermogravimetric analysis (TGA), the permittivity method, and the dilatometric method (Osipov 2012). Although these methods embody the continuous enrichment and deepening of test techniques and provide a theoretical and technical basis for the quantitative study of bound water, they have disadvantages (Smith and Vesilind 1995). In recent years, NMR has been gradually applied in the field of geotechnical engineering due to its non-destructive nature, high-efficiency and other advantages (Kleinberg *et al.* 1994, Strange *et al.* 1993). NMR can be used to detect the local structure of the rock matrix (Gallegos and Smith 1988) and identify the formation and decomposition of clathrate hydrate (Ripmeester *et al.* 2016). Ma *et al.* (2020) combined with the water distribution obtained by NMR test, discussed the variation rule for bound water and free water during drying–wetting cycles, and obtained that the maximum T_2 value of bound water (0.98 ms). Although research on the shear strength of compacted loess under different states is more abundant, few studies on the influence of bound water and free water content on soil shear strength under varying water content is lacking.

Based on the above considerations, direct shear tests of compacted loess with varying water content were carried out in this study, and the variation of shear strength and shear strength parameters with water content was analyzed. Morphology of compacted loess at different dry water contents observed by ESEM. The mass of bound water and free water in the samples with varying water content was quantified using NMR. Finally, a linear regression analysis was used to examine the influence of bound water and free water on soil shear strength parameters.

2. materials and methods

2.1 Loess samples

The loess specimens in this study were collected from a foundation pit within a loess Plateau in Yan'an City, China. A total of 85 loess samples (7.0-7.5 m depth) with a size of 20×20×40 cm were collected in the study area (latitude 35°42′46.09″ N, longitude 109°26′0.10″ E). Loess samples are classified as Malan loess. Physical properties of specimens were determined following the relevant ASTM standard (ASTM 2006) test methods. According to the XRD pattern of the original loess (Fig. 1), the quantitative mineralogical composition was calculated. The underlying physical parameters and mineralogical composition for the loess samples are listed in Table 1.

2.2 Preparation of test samples

After collection, the loess samples were prepared as follows. Firstly, the original loess was crushed using a wooden hammer until all aggregates are destroyed. The obtained material was passed through a 2 mm sieve and oven-dried at 105°C for eight hours. Next, the amount of deionized water calculated from Eq. (1) was gradually added to the samples using a spray bottle until the water content reached target value

$$m_w = \frac{0.01\times(w-w_0)}{1+0.01w_0}\times m_0 \quad (1)$$

where m_w is the mass of deionized water added, m_0 the mass of the soil sample after drying, w is the target water content, and w_0 is the initial water content.

Specimens were then thoroughly sealed within plastic film and placed into a humidity chamber for water homogenization for approximately 48 hours at room temperature. Finally, the samples were compacted directly in an oedometer cell. The final samples had a height of 20 mm, diameter of 61.8 mm, dry density of 1.55 g/cm^3, and 3%, 5%, 7%, 10%, 12%, 14%, 16.1% (plastic limit), 19%, 22%, 25%, 28.9% (liquid limit), 31%, and 33.5% (saturated) water content, respectively.

2.3 Shear test

To study the effect of compacted loess with different dry densities on shear strength, a strain-controlled direct shear

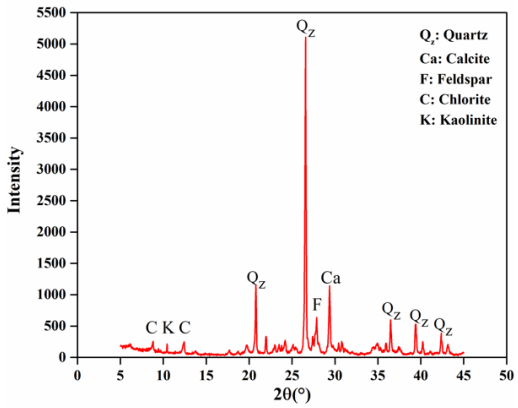

Fig. 1 XRD pattern of the original loess sample

Table 1 Physical properties of the loess analyzed in this study

Quantity	value
In situ density(g/cm^3)	1.35~1.42
Natural water content (%)	10
Specific gravity	2.71
Plastic limit (ω_P/%)	16.1
Liquid limit (ω_L/%)	28.9
Optimal water content w (%)	14.1
Maximum dry density (g/cm^3)	1.74
Quartz Content (%)	45.2 %
Feldspar Content (%)	21.0 %
Calcite Content (%)	15.5 %
Chlorite Content (%)	8.0 %
Kaolinite Content (%)	5.8 %
Illite Content (%)	4.5%

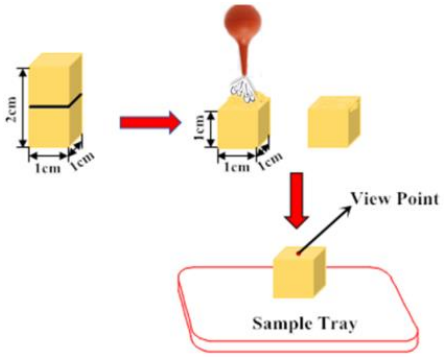

Fig. 2 Observed surface in samples

apparatus was used to apply four different vertical pressures to loess specimens with the same water content. The vertical pressures were 50 kPa, 100 kPa, 150 kPa, 200 kPa, and the shear rate is 0.8 ~ 1.2 mm/min to reduce the loss of soil samples within 3 ~ 5 min. At each pressure level, the shear strength of the sample reached the peak strength, and for those samples without significant peaks, a strain-hardening stress-strain curve corresponding to a strength of 4 mm was observed. All experiments were conducted in triplicate.

2.4 SEM test

Cubic sticks, having the dimensions of approximately 1 cm × 1 cm × 2 cm (length × width × height, were trimmed out from the central part of the loess samples after the drying-wetting cycles. Before scanning, the soil sticks were slightly fractured by hand at about 1 cm height and the new surface was used to examine the microstructure of the samples. Fig. 2 shows the surface of the samples by the ESEM. Then, half the stick was stuck to the shooting pad for sputter coating with platinum (Pt) in an ion sputtering equipment, using electron-conductive tape without disturbing the fractured plane.

2.5 NMR test

Geophysical NMR methods were used to analyze the water distributions of loess samples using MacroMR12-150H-1. It is well known that (i) the amplitude of the ^{1}H protons NMR signal in water molecules of the loess sample is proportional to the water content, and (ii) relaxation times (T_2) provide information on pore size distributions when the sample is placed in a magnetic field and then excited using a brief pulse of radio frequency (RF) energy (Costabel and Yaramanci 2013, Howard and Kenyon 1992). Relaxation time (T_2) is the transverse relaxation time of the pore water among the loess particles as measured by a Carr-Purcell-Meiboom-Gill (CPMG) sequence. T_2 is a measure of the rate at which the precession of hydrogen nuclei in the formation pore water gradually decay in the presence of an inhomogeneous magnetic field, which can be used to analyze distributions within loess samples. For loess samples, T_2 can be obtained from Eq. (2), based on the NMR relaxation mechanisms (Bleam 1991)

$$\frac{1}{T_2}=\frac{1}{T_{2B}}+\frac{1}{T_{2S}}+\frac{1}{T_{2D}} \tag{2}$$

where, T_{2B} is the bulk water relaxation time, T_{2S} is the surface-enhanced relaxation time at the pore walls, and T_{2D} is the diffusion relaxation time and accounts for the transverse relaxation in an inhomogeneous magnetic field. For water, T_{2B} is much larger than T_{2S} and T_{2D}; therefore, the effect of T_{2B} on T_2 can be ignored. For pore water in a porous loess, the T_2 of pore water is directly related to the internal pore structure of the loess

$$\frac{1}{T_2}=\frac{1}{T_{2S}}=\rho\frac{S}{V}=\rho\frac{\alpha}{r} \tag{3}$$

where ρ (expressed in general in μm/s) is the surface relaxivity coefficient, characterizing the magnetic interactions at the water-loess particle interface, and S/V is the ratio of the pore surface area S to the pore water volume V. S/V is proportional to the reciprocal of the pore radius r, expressed as $\frac{\alpha}{r}$. The geometry factor α in Eq. (3) depends on the pore shape, for example, α=1 for planar pores, α=2 for cylindrical pores, and α=3 for spherical pores. In this study, we assume that the pore structure is composed of cylindrical pores. Hence, Eq. (3) reads

$$\frac{1}{T_2}=\rho\frac{\alpha}{r}=\rho\frac{2}{r} \tag{4}$$

or

$$T_2=\frac{1}{2\rho}r \tag{5}$$

Therefore, the T_2 distribution is normalized to the sum of all amplitudes. Each amplitude then represents the proportion of water corresponding to the water relaxation time (the decay of the NMR signal), meaning that the smaller the pore, the smaller the T_2 value, that is, the adsorptive water or the water in the smaller pores relaxes faster than the free water or the capillary water within larger pores. After the samples equilibrated at the given relative temperature and humidity, the samples were placed in the NMR instrument, and the measurement of NMR signal strength was controlled using software.

2.6 Statistical analysis

The shear strength of both saturated and unsaturated soil can be defined as the maximum internal resistance of soil on the failure plane per unit area under internal or external stress. Therefore, the calculation method of saturated soil can be used to evaluate the shear strength of unsaturated soil (Khalili *et al.* 2004). The calculation of soil shear strength in this study is based on the Mohr-Coulomb law (Sarkar *et al.* 2016), which is given as follows

$$\tau_f = c' + (\sigma - u_w)_f tan\phi' \tag{6}$$

where τ_f is the soil shear strength, kPa; c′ is the soil effective cohesion force, kPa; $(\sigma - u_w)_f$ is the effective normal stress acting on the shear plane, kPa; and ϕ' is the effective angle of internal friction for a saturated soil, °.

Linear regression analysis is commonly used to understand the extent and direction of one or more variables a effecting another variable and analyze how the dependent

variable (y) changes relative to the independent variables (x_i) change (Ebrahimi *et al.* 2018). A multiple linear regression analysis model as follows

$$y = \beta_0 + \beta_1 x_1 + \cdots + \beta_k x_k + \xi \quad (7)$$

where, $x_1 \ldots x_k$ are non-random variables; y is the random dependent variable; $\beta_0 \ldots \beta_k$ are the regression coefficients; ξ is the residual, i.e., the prediction error.

If the experiment makes n observations of y and x, and gets n groups of observations $y_i, x_{1i} \ldots, x_{ki}$ $(i = 1, 2, \cdots, n)$, it satisfies the following relationship

$$y_i = \beta_0 + \beta_1 x_{1i} + \cdots + \beta_k x_{ki} + \xi_i \quad (8)$$

The matrix can be expressed as

$$y = \begin{bmatrix} y_1 \\ y_2 \\ \vdots \\ y_n \end{bmatrix}, \quad x = \begin{bmatrix} 1 & x_{11} & \cdots & x_{k1} \\ 1 & x_{12} & & x_{k2} \\ \vdots & & \ddots & \vdots \\ 1 & x_{1n} & \cdots & x_{kn} \end{bmatrix}, \quad \beta = \begin{bmatrix} \beta_0 \\ \beta_1 \\ \vdots \\ \beta_k \end{bmatrix}, \quad \xi = \begin{bmatrix} \xi_1 \\ \xi_2 \\ \vdots \\ \xi_n \end{bmatrix}$$

Therefore, the model can be written as

$$y = X\beta + \xi \quad (9)$$

Under the normal assumption, if X is full rank, then the least square estimation of the linear regression model parameters is

$$\hat{\beta} = (x^T x)^{-1} x^T y \quad (10)$$

Thus, the estimated value of y is

$$\hat{y} = x\hat{\beta} \quad (11)$$

The residual vector is $e = y - \hat{y} = y - X\hat{\beta}$; therefore, the least square estimate of the random error variance $\hat{\sigma}^2$ is

$$\hat{\sigma}^2 = \frac{e^T e}{n-k-1} \quad (12)$$

After the estimated values of the regression model parameters are obtained, a significance test of the regression equation and regression coefficient is needed.

(1) The significance test of regression equation

$$F = \frac{SSR/k}{SSE/(n-k-1)} \sim F(k, n-k-1) \quad (13)$$

where $SSR = \sum_{i=1}^{n} (\hat{y}_i - \bar{y})^2$ is the sum of regression squares; $SSE = \sum_{i=1}^{n} (y_i - \hat{y}_i)^2$ is the sum of residuals squares. For a given significance level p, the rejection domain of the test is $F > F_p(k, n-k-1)$.

(2) The significance test of regression coefficient

$$F = \frac{SSE_j/k}{SSE/(n-k-1)} \sim F(1, n-k-1) \quad (14)$$

where SSE_j is the sum of residuals squares without x_j. For a given significance level p, the rejection domain of the test is $F > F_p(1, n-k-1)$.

It can also use test statistics

$$t_j = \frac{\hat{\beta}_j}{\hat{\sigma}\sqrt{c_{jj}}} \sim t\,(n-k-1) \quad (15)$$

where, for a given significance level p, the rejection domain of the test is $|t_j| > t_{p/2}(n-k-1)$.

Here, linear regression analysis is the square root of the mean of the squared error between the value predicted from an estimate or model equation and the value observed in a real soil environment. Linear regression analysis enables checking the difference between predicted values, values from real soil experiment, and observation results (Kim *et al.* 2020). Furthermore, the correlation and suitability of regression model results and direct experiment results were evaluated. In this study, correlation and regression analyses were performed using Statistical Product and Service Solutions (SPSS) software as statistical analysis, and the shear strength was estimated from the results of free water and bound water.

3. Results and discussion

3.1 Effects of water content on shear strength

Fig. 3 presents the representative peak shear strength envelopes for specimens with different initial water contents. As water content increases, shear strength gradually decreases. For a vertical pressure of 50 kPa, the decrease in shear strength from the initial value (shear strength at a water content of 3%) is 11.04%, 21.73%, 46.19%, 55.69%, 67.47%, 74.47%, 78.51%, 81.45%, 86.31%, 89.46%, 92.22%, and 95.15%, for water contents of 5%, 7%, 10%, 12%, 14%, 16.1%, 19%, 22%, 25%, 28.9%, 31%, and 33.5%, respectively. A decrease of 12.28%, 24.64%, 40.57%, 53.15%, 62.17%, 71.20%, 74.84%, 77.82%, 82.48%, 85.60%, 88.40%, and 92.59% is obtained for the shear strength corresponding to a vertical pressure of 100 kPa. For a vertical pressure of 150 kPa, the relative decrease in shear strength is 11.19%, 22.80%, 42.15%, 51.29%, 60.45%, 67.35%, 70.60%, 73.52%, 77.72%, 80.69%, 83.46%, and 85.14%, for water contents of 5%, 7%, 10%, 12%, 14%, 16.1%, 19%, 22%, 25%, 28.9%, 31%, and 33.5% respectively. A decrease of 12.71%, 22.33%, 38.78%, 48.56%, 56.20%, 62.59%, 65.43%, 68.33%, 72.08%, 74.91%, 77.67%, and 81.93% is obtained for the shear strength corresponding to a vertical pressure of 200 kPa. The intercept of the peak shear strength envelope with the y-axis and the angle between the shear strength envelope and the x-axis are the cohesion and internal friction angles of shear strength parameters, respectively. The changes in cohesion and internal friction angle of compacted loess with increasing water content are shown in Fig. 4. The cohesion and internal friction angle decrease with increasing water content, and the decreasing rate has a sudden change at a certain water content. This sudden change is due to a change in water form within the loess. The forms of water with loess are primarily divided into bound water and free water. The humidification process of compacted loess is divided into a low-water content zone (water content is 3%, 5%, 7%, 10%, 12%, and 14%) and high-water content zone (water content is 16.1%, 19%, 22%, 25%, 28.9%, 31%, and 33.5%). The cohesion and internal friction angles in the two zones were fitted linearly.

The x-axis coordinate of the cohesion at the intersection point of the low and high-water content zone is 15.2%, and

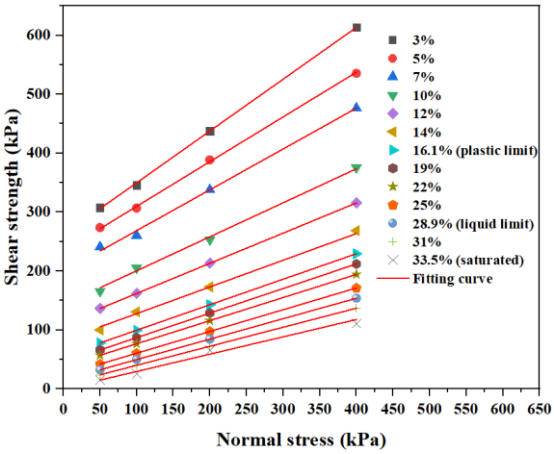

Fig. 3 Peak shear strength envelopes of the samples

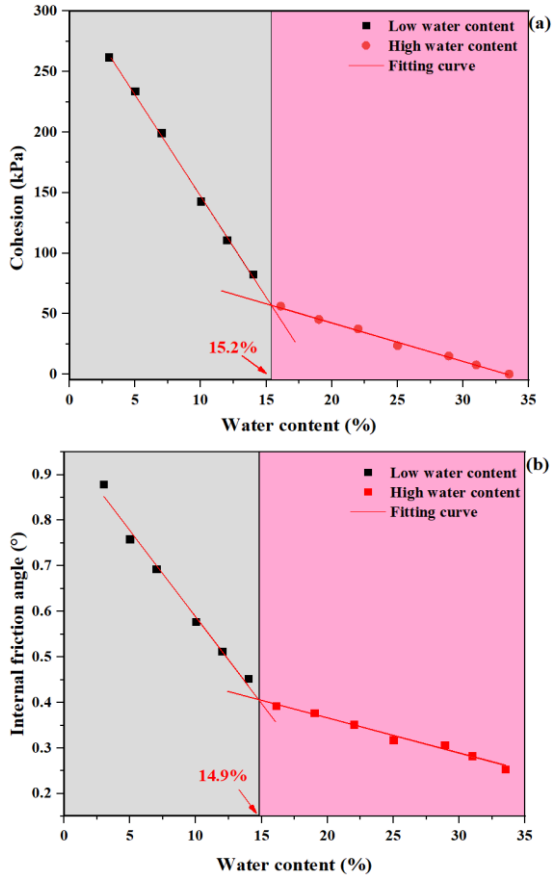

Fig. 4 Relationship between shear strength parameters and water content of the compacted specimens (a) cohesion; (b) Internal friction angle

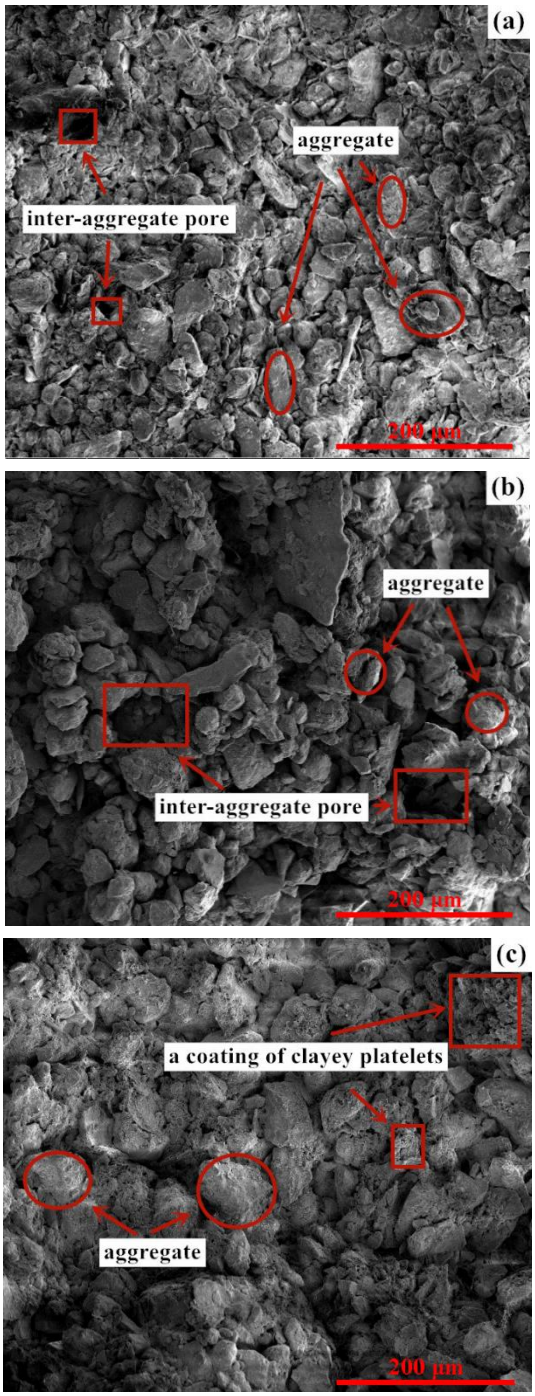

Fig. 5 Morphology of compacted loess ((a) water content 5%, (b) water content 16.1% and (c) water content 22%)

the intersection point of the internal friction angle is 14.9%. Therefore, the intersection points of cohesion and internal friction angle are practically the same for the high and low water content zones. The average value is 15.05%, which is taken as the threshold value of free water just generated in the process of humidification. Therefore, when the water content is less than 15.05%, the water in the compacted loess is in the form of bound water, and when the water content is greater than 15.05%, the water in the compacted loess is in the form of bound water and free water.

3.2 Morphology of compacted loess under different water content

The fabric resulting from different water contents was investigated with SEM observations, which exhibited differential aggregations of loess particles (Fig. 5). Figs. 5(a)-5(c) show the surface morphology of compacted loess with 5%, 16.1 and 22% water content, respectively. Fig. 5(a) demonstrates a dominant proportion of aggregates with diameters of several tens of micrometers, and also indicates the small size of aggregates compared to the wet specimen

(Fig. 5(c)). Meanwhile, most aggregates are quite clean, few aggregates are coated clay aggregates. Fig. 5(b) displays that as the water content increases, the aggregate size becomes larger and the number of inter-aggregate pores in the compacted loess structure increase. Fig. 5(c) presents that the clay in the compacted loess forms a matric that envelops around the surface of the aggregates and fills the inter-aggregates pores. Thus, in this case, it can be observed that the whole picture is more veiled by a coating of clayey platelets, which is not evident in Figs. 5(a) and 5(b). Also, most of the inter-aggregate pores found in the low water content samples are no longer evident.

3.3 Water distribution

Fig. 6 shows the T_2 distribution curves determined using the NMR technique for loess samples with different water contents. As discussed in Section 2.4, NMR signal intensity is proportional to water content, which is related to pore abundance. The x-axis represents the relaxation times, which are proportional to pore radius. The y-axis represents the water content within the pores. Results show that the T_2 distribution of all samples is unimodal and primarily distributed from 0.026 ~ 38.72 ms. With increasing water content, the peak area of loess samples increases gradually (Tian *et al*. 2018), but interestingly, the water filling of the pores is not done all at once. Even at low water content, there will still be some water in the relatively large pores. For example, for a loess sample with a water content of 5%, the pores corresponding to a T_2 of 0.2 ms are not completely saturated, but relatively large pores corresponding to a T_2 of 0.4 ms are present within the sample. This may be because the clay particles an electric field in water. Water molecules are polar molecules, and positive and negative charges are distributed at opposite ends of the water molecule. Therefore, water will be attracted to the particles surface of the relatively large pores for adsorption. When water content further increases, the free water in the void gradually increases, so that the pores are completely filled. Therefore, the loess sample is not strictly filled sequentially from micropores to macropores during the wetting process, and some water will fill the relatively large pores in the form of bound water. When the compacted loess is in the low water content zone, the T_2 relaxation time ranges from 0.01 ms to 1.58 ms. However, with increasing water content up to 16.1% (plastic limit), the maximum T_2 relaxation time increases to 2.1 ms, indicating that free water begins to exist in the compacted loess. Thus, the threshold water content between bound water and free water is slightly below the plastic limit. This is the same result as discussed in 3.1. By combining the T_2 distributions obtained from NMR, one can define a T_2 relaxation time of 1.58 ms as the boundary point for bound water distribution without free water. During loess sample saturation, the T_2 at peak (the value of T_2 at the maximum NMR signal) shifts rightward.

Fig. 7(a) shows the NMR intensity corresponding to the loess samples containing different amounts of water, which shows a good linear relationship. The equation is as follows

$$I = 2975m_w + 4.89 \quad (16)$$

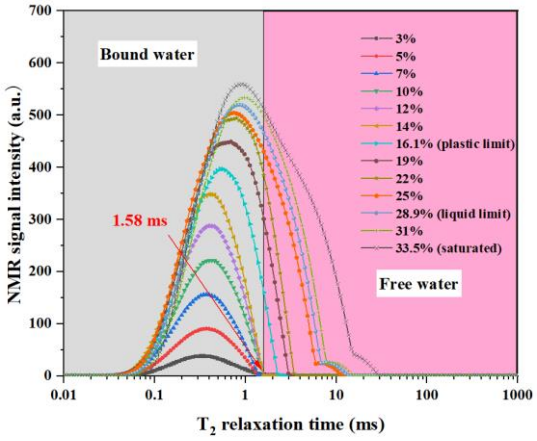

Fig. 6 T_2 distribution curves for different water contents

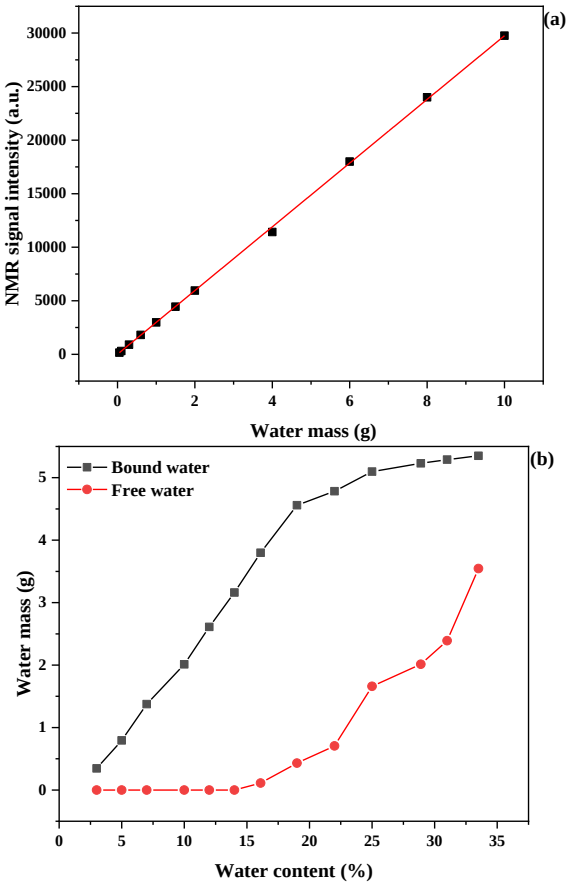

Fig. 7(a) Relationship between NMR signal intensity and water mass; (b) Mass of bound water and free water for samples with varying water content

where I is the NMR signal intensity; m_w is the mass of water in the sample. The bound water and free water for different water contents can be quantified (Fig. 7(b)). In the low-water content zone, the bound water increases linearly with increasing water content, while free water does not exist in the sample. However, when the water content reaches the high-water content zone, free water begins to appear in the compacted loess, and the growth rate of bound water decreases, while the growth rate of free water gradually increases.

Table 2 Statistical results of cohesion and internal friction angle using linear regression analysis of loess samples

Soil Variable		Unstandardized coefficients		Standardized coefficients	t-value	Significance Probability, p
		B	Standard Error	Beta		
Cohesion (kPa)	(Constant)	265.277	10.251		25.879	0.000
	Bound water w_b (g)	-52.161	3.600	-1.063	-14.489	0.000
	Free water w_f (g)	7.819	5.559	0.103	1.407	0.190
	F			205.241***		
	R^2			0.976		
Internal friction angle (°)	(Constant)	0.836	0.032		26.209	0.000
	Bound water w_b (g)	-0.103	0.011	-1.037	-9.195	0.000
	Free water w_f (g)	0.014	0.017	0.090	0.800	0.442
	F			83.921***		
	R^2			0.944		

Note: *, P<0.05; ** , P<0.01; ***, P<0.001; w_f is free water

3.4 Influence of water distribution on shear strength parameters

In order to examine the influence of bound water and free water on the shear strength parameter of loess samples, a linear regression analysis was conducted to test loess samples with varying water content. Linear regression analysis was conducted on loess samples with varying water content to determine properties effecting shear strength, cohesion, and internal friction angle. A linear regression analysis of the loess was used for bound water and free water, and the regression equation was established to estimate the cohesion and internal friction angle (Table 2).

The F values of cohesion and internal friction angle are 205.241 and 83.921, and the p values are both less than 0.001, indicating that the independent variable has a significant effect on the dependent variable. The R^2 values of the linear regression analysis model for cohesion and internal friction angle are 0.976 and 0.944, respectively, indicating that the explanatory power of bound water and free water for cohesion is 0.976, and the explanatory power of internal friction angle is 0.944. The regression coefficient and significance test show that free water (B=7.819, t=1.407, p= 0.190> 0.05) has no significant effect on the cohesion of the dependent variable. However, bound water (B=-52.161, t=-14.489, P < 0.001) had a significant negative effect on the cohesion of the dependent variable. Using the same analytical method, it can be concluded that free water (B=0.014 , t=0.800, p=0.442 > 0.05) has no significant effect on internal friction angle, but bound water (B=-0.103 , t=-9.195, p < 0.001) has a significant negative effect on internal friction angle. Therefore, bound water has a significant negative effect on shear strength, but free water has no significant effect on shear strength. The regression equation between shear strength parameters and bound water is finally obtained, as follows

$$c = 265.277 - 52.161 w_b \tag{17}$$

$$\phi = 0.836 - 0.103 w_b \tag{18}$$

where c is cohesion of loess, ϕ is internal friction angle of loess, and w_b is bound water.

4. Conclusions

In this paper, shear strength and NMR curves of compacted loess samples with varying water content were measured. The conclusions drawn from this study are as follows:

- The shear strength and shear strength parameters decrease with increasing water content. Based on changes in cohesion and internal friction angle, the water content can be divided into a high-water content zone and low-water content zone with a boundary water content of 15.05%.
- With increasing water content, the aggregates size of the compacted loess gradually increases. Meanwhile, the clay in the compacted loess forms a matric that envelops around the surface of the aggregates and fills the inter-aggregates pores.
- The mass of bound water and free water for different water contents can be quantitatively determined using the NMR curve. The boundary point for bound water distribution without free water was defined as a T_2 relaxation time of 1.58 ms.
- The influence of free water and bound water as independent variables on shear strength parameters was explored through linear regression analysis. Bound water had a significant and negative correlation

with shear strength. However, free water had no significant effect on shear strength parameters. Finally, the equation for bound water and shear strength parameters was obtained, which is significant for future research on shear strength mechanisms.

Acknowledgments

The authors gratefully acknowledge the China Postdoctoral Science Foundation (Grant no. 2019T120873 and Grant no. 2018M631117), Postdoctoral Research Project in Shaanxi Province (Grant no. 2018BSHGZZHQYXMZZ26), the Key Program of the National Natural Science Foundation of China (Grant no. 41931285), and the key research and development program of Shaanxi Province (Grant no. 2019ZDLSF05-07).

References

Assallay, A.M., Rogers, C.D.F. and Smalley, I.J. (1997), "Formation and collapse of metastable particle packings and open structures in loess deposits", *Eng. Geol.*, **48**(1-2), 101-115. https://doi.org/10.1016/S0013-7952(97)81916-3.

ASTM (2006), Annual Book of ASTM Standards. *ASTM International, West Conshohocken, Pa.*

Bakir, N., Abbeche, K. and Panczer, G. (2017), "Experimental study of the effect of the glass fibers on reducing collapse of a collapsible soil", *Geomech Eng.*, **12**(1), 71-83. https://doi.org/10.12989/gae.2017.12.1.071.

Bleam, W.F. (1991), "Soil science applications of nuclear magnetic resonance spectroscopy", *Adv. Agron.*, **32**. 91-155. https://doi.org/10.1016/S0065-2113(08)60579-9.

Carey, J.M., McSaveney, M.J. Petley, D.N. (2017), "Dynamic liquefaction of shear zones in intact loess during simulated earthquake loading", *Landslides.*, **14**, 789-804. https://doi.org/10.1007/s10346-016-0746-y.

Costabel, S. and Yaramanci, U. (2013), "Estimation of water retention parameters from nuclear magnetic resonance relaxation time distributions: Estimation of water retention parameters from NMR", *Water Resour. Res.*, **49**(4), 2068-2079. https://doi.org/10.1002/wrcr.20207.

Derbyshire, E., Dijkstra, T.A., Smalley, I.J. and Li, Y. (1994), "Failure mechanisms in loess and the effects of moisture content changes on remoulded strength", *Quat. Int.*, **24**, 5-15. https://doi.org/10.1016/1040-6182(94)90032-9.

Dijkstra, T.A., Rogers, C.D.F., Smalley, I.J., Derbyshire, E., Li, Y.J. and Meng, X.M. (1994), "The loess of north-central China: Geotechnical properties and their relation to slope stability", *Eng. Geol.*, **36**(3-4), 153-171. https://doi.org/10.1016/0013-7952(94)90001-9.

Ebrahimi, M., Sarikhani, M.R., Safari Sinegani, A.A., Ahmadi, A. and Keesstra, S. (2019), "Estimating the soil respiration under different land uses using artificial neural network and linear regression models", *CATENA*, **174**, 371-382. https://doi.org/10.1016/j.catena.2018.11.035.

Gallegos, D.P. and Smith, D.M. (1988), "A NMR technique for the analysis of pore structure: Determination of continuous pore size distributions", *J Colloid Interf. Sci.*, **122**(1), 143-153. https://doi.org/10.1016/0021-9797(88)90297-4.

Gu, T., Wang, J., Wang, C., Bi, Y., Guo, Q. and Liu, Y. (2019), "Experimental study of the shear strength of soil from the Heifangtai platform of the loess plateau of China", *J. Soils Sediments.*, **19**, 3463-3475. https://doi.org/10.1007/s11368-019-02303-9.

Guo, Y., Ni, W. and Liu, H. (2021), "Effects of dry density and water content on compressibility and shear strength of loess", *Geomech. Eng.*, **24**(5), 419-430. https://doi.org/10.12989/gae.2021.24.5.419.

Houston, S.L., Houston, W.N., Zapata, C.E. and Lawrence, C. (2001), "Geotechnical engineering practice for collapsible soils, in: (Ed., Toll, D.G.), unsaturated soil concepts and their application in geotechnical practice", *Spr Nether.*, 333-355. https://doi.org/10.1007/978-94-015-9775-3_6.

Howard, J.J. and Kenyon, W.E. (1992), "Determination of pore size distribution in sedimentary rocks by proton nuclear magnetic resonance", *Mar Pet Geol.*, **9**(2), 139-145. https://doi.org/10.1016/0264-8172(92)90086-T.

Khalili, N., Geiser, F. and Blight, G.E. (2004), "Effective stress in unsaturated soils: Review with mew evidence", *Int. J. Geomech.*, **4**(2), 115-126. https://doi.org/10.1061/(ASCE)1532-3641(2004)4:2(115).

Kie (1988), "Fundamental properties of loess from Northwestern China", *Eng. Geol.*, **25**(2-4), 103-122. https://doi.org/10.1016/0013-7952(88)90022-1.

Kim, K.S., Kim, M.I., Lee, M.S. and Hwang, E.S. (2020), "Regression equations for estimating landslide-triggering factors using soil characteristics", *Appl. Sci.*, **10**, 3560. https://doi.org/10.3390/app10103560.

Kleinberg, R.L. (1994), "Pore size distributions, pore coupling, and transverse relaxation spectra of porous rocks", *MAGN Reson. Imaging*, **12**(2), 271-274. https://doi.org/10.1016/0730-725X(94)91534-2.

Low, P.F. (1979), "Nature and properties of water in montmorillonite-water systems", *Soil Sci Soc Am J.*, **43**(4), 651-658. https://doi.org/10.2136/sssaj1979.03615995004300040005x.

Ma, T., Wei, C., Yao, C. and Yi, P. (2020), "Microstructural evolution of expansive clay during drying–wetting cycle", *Acta Geotech.*, **15**, 2355-2366. https://doi.org/10.1007/s11440-020-00938-4.

Markgraf, W., Horn, R. and Peth, S. (2006), "An approach to rheometry in soil mechanics—Structural changes in bentonite, clayey and silty soils", *Soil Tillage Res.*, **91**(1-2), 1-14. https://doi.org/10.1016/j.still.2006.01.007.

Mei, Y, Hu, C.M., Yuan, Y.L., Wang, X.Y. and Zhao, N. (2016), "Experimental study on deformation and strength property of compacted loess", *Geomech. Eng.*, **11**(1), 161-175. https://doi.org/10.12989/gae.2016.11.1.161.

Osipov, V.I. (2012), "Nanofilms of adsorbed water in clay: Mechanism of formation and properties", *Water Resour.*, **39**, 709-721. https://doi.org/10.1134/S009780781207010X.

Pye, K. (1995) "The nature, origin and accumulation of loess", *Quaternary Sci. Rev.*, **14**(7-8), 653-667. https://doi.org/10.1016/0277-3791(95)00047-X.

Ripmeester, J.A. and Alavi, S. (2016), "Some current challenges in clathrate hydrate science: Nucleation, decomposition and the memory effect", *Curr. Opin Solid St M.*, **20**(6), 344-351. https://doi.org/10.1016/j.cossms.2016.03.005.

Rost, K.T. (2001), "Late Holocene loess deposits and dust accumulation in the alpine meadow belt of the Wutai Shan, China", *Quat. Int.*, **76-77**, 85-92. https://doi.org/10.1016/S1040-6182(00)00092-6.

Sarkar, S., Roy, A.K. and Raha, P. (2016), "Deterministic approach for susceptibility assessment of shallow debris slide in the Darjeeling Himalayas, India", *Catena* **142**, 36-46. https://doi.org/10.1016/j.catena.2016.02.009.

Smalley, I. and Rogers, C. (1996), "Loess: The yellow earth", *Geo. Today.*, **12**, 186-193. https://doi.org/10.1046/j.1365-2451.1996.00015.x.

Smith, J.K. and Vesilind, P.A. (1995), "Dilatometric measurement of bound water in wastewater sludge", *Water Res.*, **29**(12), 2621-2626. https://doi.org/10.1016/0043-1354(95)00144-A.

Strange, J.H., Rahman, M. and Smith, E.G. (1993), "Characterization of porous solids by NMR", *Phys. Rev. Lett.*, **71**, 3589-3591. https://doi.org/10.1103/PhysRevLett.71.3589.

Tian, H., Wei, C., Lai, Y. and Chen, P. (2018), "Quantification of water content during freeze-thaw cycles: A nuclear magnetic resonance based method", *Vadose Zone J.*, **17**(1), 160124. https://doi.org/10.2136/vzj2016.12.0124.

Wen, B.P. and Yan, Y.J. (2014), "Influence of structure on shear characteristics of the unsaturated loess in Lanzhou, China", *Eng. Geol.*, **168**, 46-58. https://doi.org/10.1016/j.enggeo.2013.10.023.

Youssef, A.M. and Maerz, N.H. (2013), "Overview of some geological hazards in the Saudi Arabia", *Environ Earth Sci.*, **70**, 3115-3130. https://doi.org/10.1007/s12665-013-2373-4.

CC